Research Article

Journal of Chemistry Letters
journal homepage: www.jchemlett.com
ISSN (online):2717-1892

Computational Modeling and Molecular dynamics Simulations of Thiazolino 2-pyridone amide analog compounds as Chlamydia trachomatis inhibitor

Emmanuel Israel Edache [a,] *, Adamu Uzairu[b], Paul Andrew Mamza[b] and Gideon Adamu Shallangwa[b]

[a] *Department of Pure and Applied Chemistry, University of Maiduguri, Borno State, Nigeria*
[b] *Department of Chemistry, Ahmadu Bello University, Zaria, Nigeria*

ARTICLE INFO

Article history:
Received
Received in revised form
Accepted
Available online

Keywords:
Chlamydia trachomatis;
thiazolino 2-pyridone amide derivative;
2D-QSAR;
CoMFA (3D-QSAR);
Partial least-square;
molecular docking;
molecular dynamic simulation

ABSTRACT

Computer-aided drug screening by 2D-QSAR, CoMFA, molecular docking, and molecular dynamics (MD) simulation may provide an effective approach to identifying promising drug repurposing candidates for Chlamydia trachomatis treatment. In this analysis, molecular descriptors were used to achieve a statistically momentous 2D-QSAR model (R^2 = 0.637; Q^2 = 0.5388). The 2D-QSAR model's robustness was considered by the internal leave-one-out cross-validated regression coefficient values (Q^2) and the training set values [(r^2-r0^2)/r^2]. Between the experimental and predicted pIC_{50} value, the overall standard deviation error of prediction (SDEP) was 0.2448, showing strong 2D-QSAR model predictability. The QSAR model was able to systematically predict anti-bacterial behavior with an R2pred value of 0.506 for the external data set 9 of the thiazolino 2-pyridone amide derivative. Comparative molecular field analysis (CoMFA (FFDSEL) Q^2_{LOO} = 0.238, R^2 = 0.943) and CoMFA (UVEPLS) (Q^2LOO = 0.553, R^2 = 0.943) were used. CoMFA (UVEPLS) had strong certification and prediction capabilities. We analyzed the binding effect of the derivatives, where compounds 29 and 31 have the least binding energy. Compounds 29 and 31 interact with main active site residues, including Glu154, Leu142, His87, Arg150, Phe151, Asn138, Gly141, His88, Ile137, Cys85 and 145, respectively, through the binding interaction modes of the molecular docking inhibitor sequence. Further molecular dynamics simulations (MD) were performed on both compounds, and their potential binding modes were explored. Glu154, Phe151, Arg150, Asn138, Gly141, Cys145, and Ile137 have been found to play a key role in stabilizing inhibitors. Besides, the prediction of a golden triangle for the series was carried out. The findings will provide useful guidance in the future for the design of new inhibitors of Chlamydia trachomatis.

1. Introduction

Chlamydia trachomatis is the most common sexually transmitted bacterial infection all around the world that can prompt barrenness and increased susceptibility to other sexually transmitted pathogens, such as HIV/AIDs [1], tumors and complications of pregnancy, as well as trachoma, a recurrent eye infection [2]. Without treatment with antibiotics, Chlamydia trachomatis infections of the female genital tract can prompt fruitlessness, a major public health concern [3]. 85 million people have received antibiotics for trachoma, a blinding eye infection that occurs in 42 countries [4], and there are more than 100 million yearly instances of sexually transmitted Chlamydia trachomatis overall [5]. There is no vaccine for Chlamydia trachomatis at present. Throughout the year's quantitative structural activity relationship (QSAR), 3D-QSAR procedures, for example, comparative molecular field analysis (CoMFA) and comparative molecular similarity indices analysis (CoMSIA) assess key structural features and aid underlying alteration in structural modification of the compounds to improve their potency [6]. A 14-membered macrolide analog against mycobacterium tuberculosis was reported by Zitouni et al. Where the 2D-QSAR was established, the inhibitory activity of the investigated macrolide derivatives was predicted and near agreement was obtained between experimental and predicted values

* Corresponding author. Tel.: +2348066776802; e-mail: edacheson2004@gmail.com

[7]. Marwaha et al. likewise revealed a high-content screen of 9,800 compounds identifying acylated sulfonamides as novel growth inhibitors of the sexually transmitted pathogen Chlamydia trachomatis [1]. The impact was bactericidal and distinct from that of sulfonamide antibiotics, as para-amino benzoic acid did not reduce efficacy. Dahlgren et al. did a statistical molecular design (SMD), quantitative structure-activity relationship (QSAR) modeling to pick up knowledge into the structural basis of the inhibitory mechanism of novel salicylidene acylhydrazides as inhibitors of type III secretion (T3S) in the Gram-negative pathogen Yersinia pseudotuberculosis [8]. Mojica and his coworker introduced a form of image-based screening with red fluorescent Chlamydia that was autonomously detected without the need for immune-staining Chlamydia by automated microscopy. The technique was applied to compounds that inhibit the growth of Chlamydia and identified Australian natural compounds that were previously defined as an antimicrobial activity in image-based screening. Besides, the approach was used over time for live-cell monitoring of Chlamydia-infected cells and visualized the growth inhibitory effect of Chlamydia cell culture infection's most active natural compound [9]. For the study of different bacteria inhibitors, a variety of in-silico, in-vitro, and in-vivo techniques have been applied. To establish more efficient ways of managing this infection and preventing the reproductive dysfunction it is associated with much more research is required to understand the balance between the immune response and the organism's development. There are few treatment options for infections with these mandatory intracellular bacteria and the most common treatment worldwide is a single dose of azithromycin, erythromycin, and doxycycline. In other human pathogenic bacteria, this protocol has preferred macrolide tolerance [10, 11] and a more selective approach would therefore be preferable. C. trachomatis readily develop resistance to antibiotics in *in-vitro* [12] and novel anti-chlamydial agents may become important in the future for the treatment of these infections. To recognize lead compounds for anti-chlamydial medication improvement, we screened a library of 46 thiazolino 2-pyridone amide derivatives for their ability to hinder Chlamydia development. In this investigation, QSAR models for thiazolino 2-pyridone amide derivatives of Chlamydia trachomatis inhibitors are provided in this report. Also, it addresses the binding mode of most activity compounds obtained through docking and MD simulation tests at the Chlamydia trachomatis binding site is examined.

2. Results and Discussion

The 2D-QSAR model created in this study was factually best fitted and along these lines was utilized for prediction of activities against strains of Chlamydia trachomatis of training and test sets (pIC_{50}) of molecules, as reported in model 1. The R^2 and Q^2 values of 0.637 and 0.539, respectively, of the model, corroborate with the criteria for a QSAR model to be highly predictive [25]. The standard error of estimate (SEE) for the model was 0.2436, which is a marker of the strength of the fit and recommended that the predicted pIC_{50} based on model 1 is solid [26].

pIC50 = 3.58996+0.21534ALogP +0.33886nHBint3 +0.25785MLogP_____Model 1

SEE = 0.2298, R^2 = 0.6374, R^2 adjusted = 0.6044, F = 19.3359, Q^2 = 0.5388, PRESS = 2.2168, SDEP = 0.2448, RMSEP = 0.2858, R^2pred = 0.506, K = 1.0213, [(r^2-r0^2)/r^2] = 0.0285, K' = 0.9771

The root means square error of prediction (RMSEP) between the experimental and predicted pIC_{50} values was 0.286, which uncover great consistency. The value of [(r^2 –r0^2)/r^2] = 0.029, which is under 0.1 specified worth [25] and in this way approve the value of the QSAR model for foreseeing the organic action (biological activity) of the external data set. Likewise, the estimations of K and K′ were 1.021 and 0.977, respectively, which are well inside the predetermined scopes of 0.85 and 1.15 [25]. The values of R^2_{pred} = 0.506 were found to be in the acceptable range [27] in this way showing the great external consistency of the QSAR model. The connection between predicted activities and the corresponding experimental activities is presented in Table 1. Williams plot (Figure 1A) [28], clearly two compounds, the training set (compound 3) and test set (compound 31) fall outside the space of the model (the warning leverage limit is 0.32). These compounds (3 and 31) have the leverage higher than the warning h* value, consequently they can be viewed as structural outliers. Fortunately, for this situation, the information anticipated by the model is acceptable, hence they are ‘‘acceptable leverage” compounds. For all the compounds in the training and test sets, their standardized residuals are more modest than three standard deviation units (±3δ). Insubria graph [29] were also used to confirm the Williams plot, we checked that most of the examined 46 compounds fell into the structural applicability domain (AD) of the QSAR model; in details, 44 compounds (96%) were inside the domain for the range of descriptors method, compound 3 and 31 (4%) fell outside the AD (Figure 1B). This permits us to think about most of our expectations as introduced by the model, and thus more reliable. The determination coefficient (R^2) of this model was 0.637, which shows the great internal prediction power of this model (Figure 1C), where the difference between the experimental and predicted are not far from each other (Figure 1D). Therefore, the results of validations steps show that the model can be delegated a decent model since according to the criteria used, it has a great interior (internal) and outer (external) quality, it is robust, it doesn’t experience chance correlation at

random, and it shows a good capacity of external predictions [30].

Table 1: 2D-QSAR and CoMFA observed and predicted activities

Methods		2D-QQSAR		CoMFA (FFDSEL)		CoMFA (UVEPLS)	
Name	Yobs	Ypred	Residuals	Ypred	Residuals	Ypred	Residuals
2	6	6.2094	-0.2094	6.065	-0.065	6.026	-0.026
3	5.301	4.9051	0.3959	5.373	-0.072	5.299	0.002
4	5.6021	5.5224	0.0797	5.575	0.0271	5.553	0.0491
5	5.6021	5.6021	0	5.507	0.0951	5.528	0.0741
7	5.6021	5.6021	0	5.505	0.0971	5.524	0.0781
8	5.6021	5.9178	-0.3157	5.519	0.0831	5.599	0.0031
9	5	4.9729	0.0271	5.159	-0.159	5.1	-0.1
10	5	5.5197	-0.5197	4.842	0.158	4.94	0.06
12	6	6.1854	-0.1854	5.913	0.087	5.979	0.021
13	6.6021	5.9967	0.6054	6.577	0.0251	6.546	0.0561
14	5.6021	5.6214	-0.0193	5.502	0.1001	5.495	0.1071
15	5.6021	5.4537	0.1484	5.609	-0.0069	5.5555	0.0471
17	5	5.3453	-0.3453	5.152	-0.152	5.09	-0.09
18	6	5.7221	0.2779	6.059	-0.059	6.072	-0.072
19	6	5.5089	0.4911	6.009	-0.009	6.01	-0.01
20	5.6021	5.6326	-0.0305	5.576	0.0261	5.66	-0.0579
22	5.6021	5.4911	0.11	5.513	0.0891	5.5061	0.0961
23	5.6021	5.4067	0.1954	5.74	-0.1379	5.631	-0.0289
24	5.6021	5.2438	0.3583	5.632	-0.0299	5.626	-0.0239
25	5.6021	5.5525	0.0496	5.566	0.0361	5.548	0.0541
27	6	5.7042	0.2958	5.696	0.304	5.717	0.283
28	5.6021	5.6905	-0.0884	5.732	-0.1299	5.757	-0.1549
29	5.6021	5.7544	-0.1523	5.633	-0.0309	5.682	-0.0799
30	5.6021	5.4898	0.1123	5.82	-0.2179	5.803	-0.2009
32	5.6021	5.5525	0.0496	5.469	0.1331	5.503	0.0991
33	5.6021	5.6559	-0.0538	5.642	-0.0399	5.651	-0.0489
34	5.6021	5.7367	-0.1346	5.535	0.0671	5.545	0.0571
35	5.6021	5.4898	0.1123	5.539	0.0631	5.588	0.0141
37	5	5.2055	-0.2055	5.054	-0.054	4.986	0.014
38	5	5.4989	-0.4989	4.956	0.044	4.998	0.002
39	5	5.0515	-0.0515	5.13	-0.135	5	0
40	5.301	5.1373	0.1637	5.427	-0.126	5.472	-0.1710
42	5.301	5.2539	0.0471	5.287	0.014	5.301	0
43	5	5.2977	-0.2977	5.044	-0.044	5.006	-0.006
44	5	5.0953	-0.0953	4.994	0.006	5.038	-0.038
45	5.6021	5.6932	-0.0911	5.584	0.0181	5.633	-0.0309
46	5.301	5.3157	-0.0148	5.313	-0.012	5.282	0.019
Test set	Yobs	Ypred	Residuals	Ypred	Residuals	PC5	Residuals
1	5.6021	5.9615	-0.3594	5.906	-0.3039	5.871	-0.2689
6	5.6021	5.6021	0	4.738	0.8641	4.705	0.8971

11	6.6021	6.0167	0.5854	6.127	0.4751	6.095	0.5071
16	5.6021	5.6204	-0.0183	5.773	-0.1709	5.787	-0.1849
21	5.6021	5.3714	0.2307	5.458	0.1441	5.445	0.1571
26	5.6021	5.6531	-0.0512	5.021	0.5811	4.921	0.6101
31	5	4.9041	0.0959	5.433	-0.4337	5.457	-0.4577
36	5.6021	5.3949	0.2072	5.437	0.1651	5.534	0.0681
41	5.6021	5.2085	0.3936	4.849	0.7531	4.977	0.6321

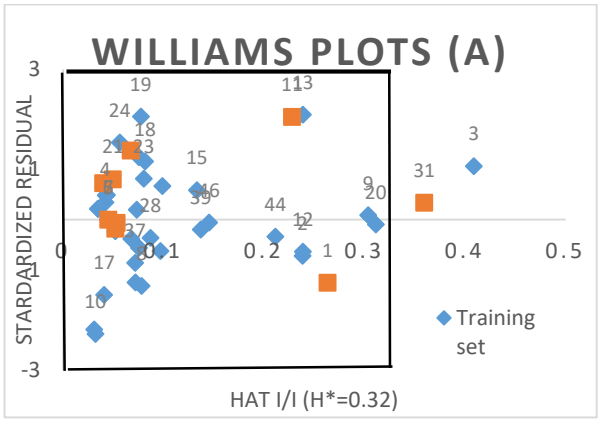

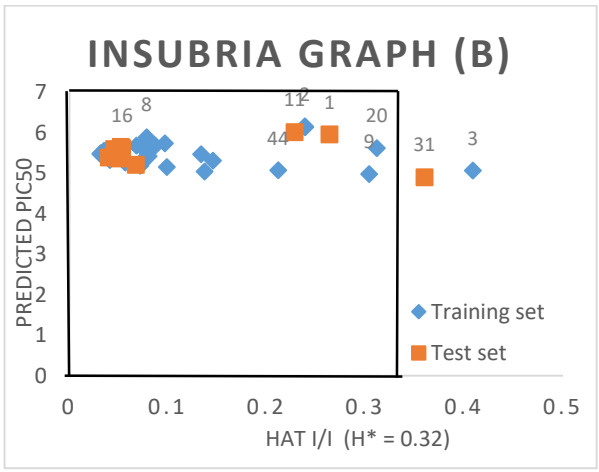

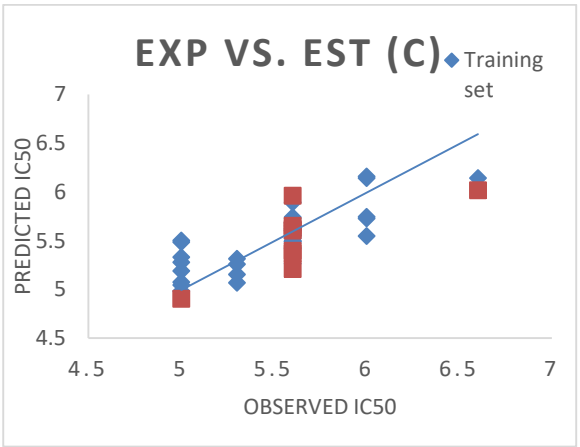

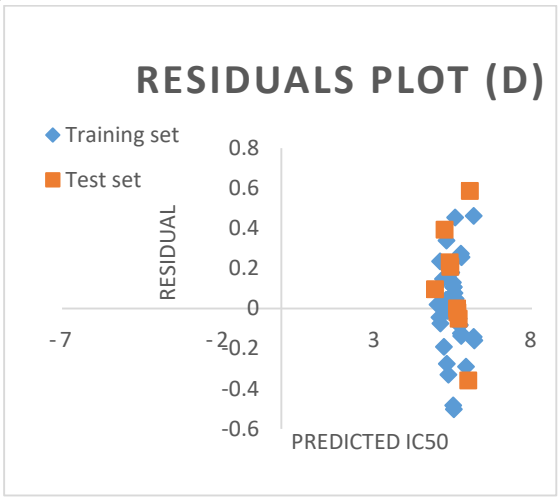

Figure 1: Diagram of the prediction comparison (A) Williams plot, (B) Insubria graph, (C) observed IC50 vs. predicted IC50, and (D) Residuals plot.

The QSAR developed indicated that Ghose-Crippen LogKow (ALogP), Count of E-State descriptors of strength for potential Hydrogen Bonds of path length 3 (nHBint3), and Mannhold LogP (MLogP) has positive values in the mean effect (MF) demonstrate that the showed descriptor contributes absolutely to the value of pIC_{50}, the more the rate of the properties (descriptor) the higher the value of pIC_{50}. In other words, increasing the ALogP (0.5%), nHBint3 (98.30%), and MLogP (1.2%) increases the extent of pIC_{50} of the thiazolino 2-pyridone amide derivatives (Table 2) by the percentage contribution. To further check the inter-correlation of descriptors, the variance inflation factor (VIF) analysis was implemented. In this model, the VIF values of these descriptors are shown in Table 2 which are less than the threshold value of 5 [26, 31], which conforms to the study that, the properties engaged in the model are not inter-correlated with one another.

Table 2: Description of selected variables are as follows:

Symbol	Name Descriptors	Mean effect	Percentage contribution (%)	VIF
ALogP (PaDEL; 2D)	Ghose-Crippen LogKow	0.2796	0.50	1.0972
nHBint3 (PaDEL = 2D)	Count of E-State descriptors of strength for potential Hydrogen Bonds of path length 3	54.5327	98.30	1.0387
MLogP (PaDEL; 2D),	Mannhold LogP	0.66380	1.20	1.0575

The 3D-QSAR model with reliable predictive ability must fulfill the accompanying conditions: leave one out cross-validation (Q^2_{LOO}) should be greater than 0.5, determination coefficient (R^2) should be greater than 0.9, the standard deviation error in estimation (SDEC) worth should be as small as could be expected under the circumstances and the F-test worth should be high as could be expected under the circumstances [32].

To more readily comprehend the underlying structural requirement of thiazolino 2-pyridone amide inhibitors, two Open3DQSAR models were developed using two distinctive variable choice strategies, named fractional factorial design (FFDSEL), where the steric and electrostatic field descriptors explain 54.0% and 46.0% of the variance, respectively (Figure 2) and UVE-PLS variable selection (UVEPLS), where the steric and electrostatic field descriptors explain 44.0% and 56.0% of the variance, respectively (Figure 3).

The measurable boundaries determined by Open3DQSAR models showed good R^2 and Q^2_{LOO} values. Looking at the measurable highlights shows that UVE-PLS variable selection created by Open3DQSAR models could provide suitable results; however, the outcomes for the UVE-PLS model (R^2 = 0.943; F-test = 102.376; Q^2_{LOO} = 0.553) are higher than those gotten from the FFDSEL (R^2 = 0.92; F-test = 71.013; Q^2_{LOO} = 0.238) variable choice technique. In this way, the UVE-PLS model is viewed as the best 3D-QSAR model. The partial least square (PLS) steric-electrostatic contour map of Open3DQSAR models of thiazolino 2-pyridone amide inhibitors is represented in Figure 3.

The red and the blue areas portray the steric bulky groups, favorable and unfavorable, respectively, to thiazolino 2-pyridone amide inhibition activity. The green contours demonstrate the regions where the presence of electropositive groups would add to expanding thiazolino 2-pyridone amide inhibitory strength, while the shapes of the yellow contours show the territories where such electro-positivity is unfavorable to biological activity.

As demonstrated in Figure 3, the red contour and green contours at the region propose a bulkier sweet-smelling bunch (aromatic group) was important to the thiazolino 2-pyridone amide inhibition activity of a ligand.

Most importantly, our Open3DQSAR study uncovers the significance of a four-atom linker at blue contour and a bulkier group at red contour for better biological potency. The observed/experimental (Yobs) and predicted/estimated (Ypred) activities along with the residual values of the training set and test set molecules are potted in Table 1.

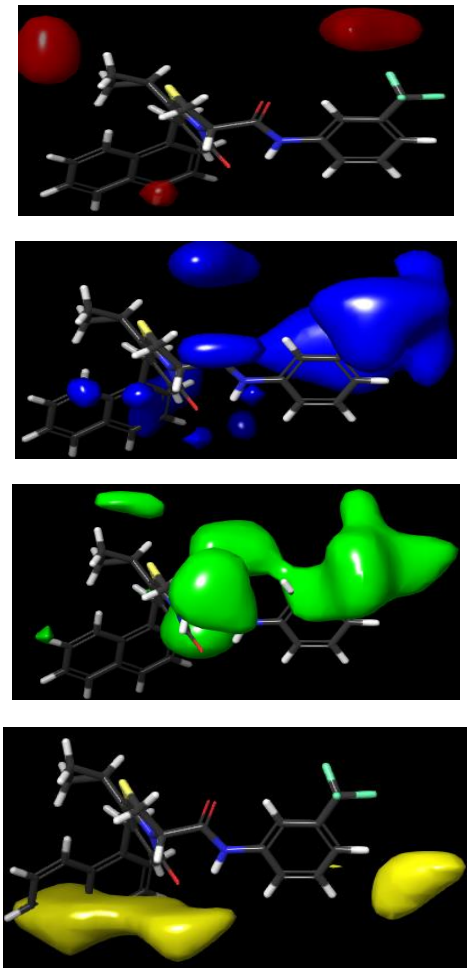

Figure 2. CoMFA (FFDSEL) contour map with reference compound 29

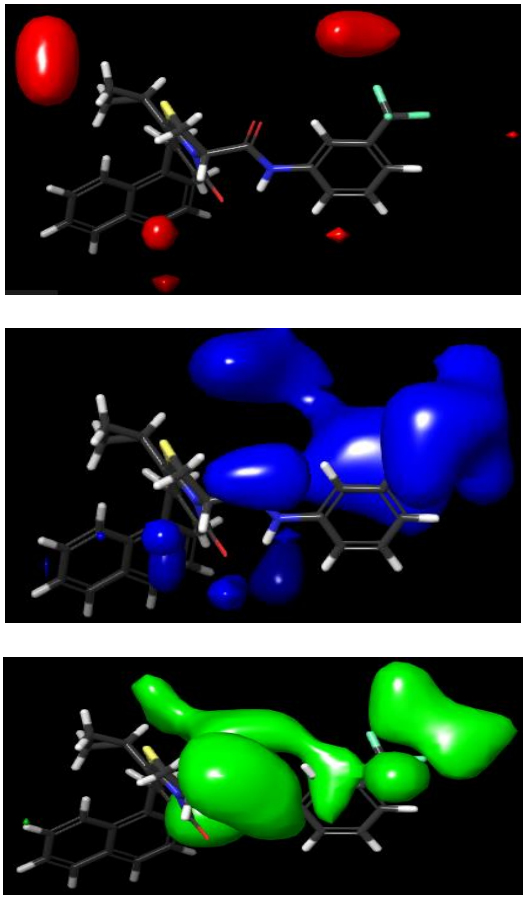

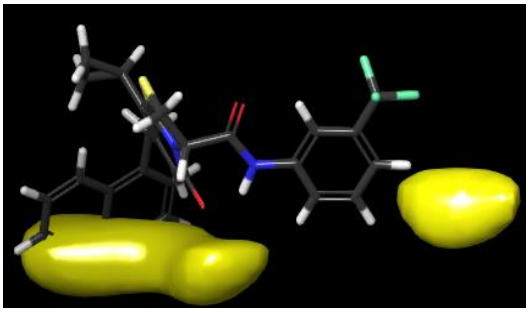

Figure 3. CoMFA (UVEPLS) contour map with reference compound 29

The docking studies were done to virtual screen the 46 compounds, screened in-prior through the determined 3D-QSAR model, just as to recognize the binding potency and poses of dynamic molecules so that to uncover the molecular mechanism of action. Before docking contemplates, the protein (PDB: 5KBC) was readied. The ligands, when docked, exhibited a few postures, orientation, and thus several configurations. Each configuration is portrayed as a consolidated score of Van der Waals forces, conventional hydrogen bonding, carbon-hydrogen bonding, hydrophobic interaction as well as other relevant parameters. The least auto dock/vina score indicates a higher chance of ligand-protein binding (Table 4). The docked ligands, namely, compound 29 and 31 gives a docking score of -8.9 kcal/mol. Both compounds were found interacting with Van der Waals forces, conventional hydrogen bonding, carbon-hydrogen bonding, and hydrophobic interaction, whereas, compound 29, form a halogen interaction with His88 amino acid. Compounds 29 and 31 showed hydrogen bond formation. Compound 31 has the highest number of interactions with the enzyme. These outcomes demonstrate that the candidate compound (ligand 31, with the highest number of interactions) showed good docking interactions in contrast with compound 29, thus indicating the high binding affinity of these hit compounds (Figure 4). The detailed docking score is shown in Table 4. The hydrogen bond interactions alongside interactive amino acid were summed up in Table 3. Furthermore, a 2D diagram was given in Figure 4 to uncover different molecular interactions. These interactions are meant by separate colors and their interpretation as presented in Figure 4.

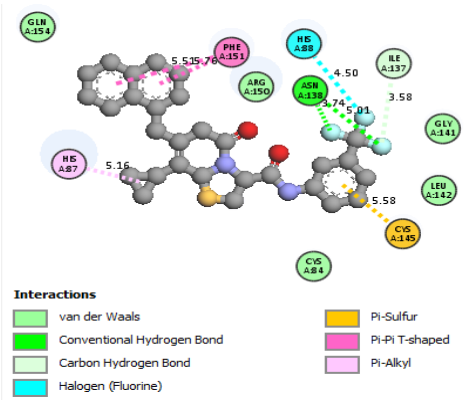

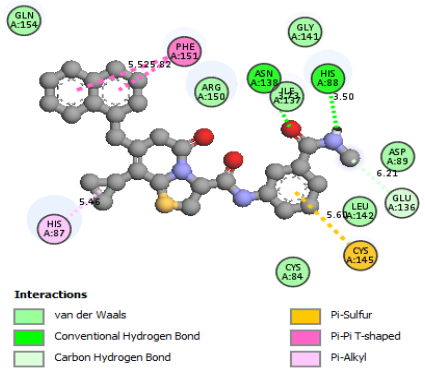

Figure 4. Finest docking poses for binding of physiological ligands to (A) compound 29 (B) compound 31

Table 3. Hydrogen bond interactions of compound 29 and 31

Compound 29	Distance	Donor Atom	Acceptor Atom
HIS87: HN - :CYS84: O	2.4866	HN	O
ASN138:HN - cpd29:F	2.3149	HN	F
LEU142: HN - ASN138: O	2.1800	HN	O
CYS145:HN -GLY141:O	2.3987	HN	O
Cpd29: H – cpd29: O	2.2507	H	O
Compound 31	Distance	Donor Atom	Acceptor Atom
HIS87: HN - CYS84: O	2.4866	HN	O
ASN138:HN - :cpd31: O	1.9752	HN	O
LEU142: HN - ASN138: O	2.1800	HN	O
CYS145: HN - GLY141: O	2.3987	HN	O
cpd31: H – cpd31: O	2.3974	H	O
cpd31: H - HIS88: O	1.8569	H	O

The MD simulations of the protein-ligand complex demonstrate the stability of the complex and permitted additional data about the binding mode of ligands. The root mean square deviation (RMSD, hydrogen bond, total energy, and temperature plot during the MD simulations are shown in Figure 5A to 5D, respectively. The simulation result layout that the RMSD is around 1.7Å (Figure 5A), total energy, and temperature fluctuate around -41,307kcal/mol, 298K, respectively after 50,000 runs. Comparing the configuration of the complex after stimulation with the docking confirmation as shown in

Figure 6. Compounds 29 and 31 assume a similar docking site with the protein but move better off in the binding pocket of the protein and this would altogether expand the binding affinity. From the results, CoMFA (UVEPLS), molecular docking, and MD simulations show a strong understanding of the structure-activity relationship and binding modes of the ligand for inhibitors of the crystal structure of Chlamydia trachomatis DsbA. The results of 3D-QSAR uncover the impact of each steric and electrostatic interaction on the bioactivity, and the docking results affirmed this outcome. At the same time, the results of molecular docking and MD simulations also uncovered some important interactions concerning the ligands and the protein. The MD simulations also explained hydrogen bond, steric, and electrostatic interaction on the ligand with the key active site residues, including Glu154, Leu142, His87, Arg150, Phe151, Asn138, Gly141, His88, Ile137, Cys85 and 145, respectively. These molecular modeling studies would give valuable data and apparatuses for our next plan and improvement of other Chlamydia trachomatis inhibitors.

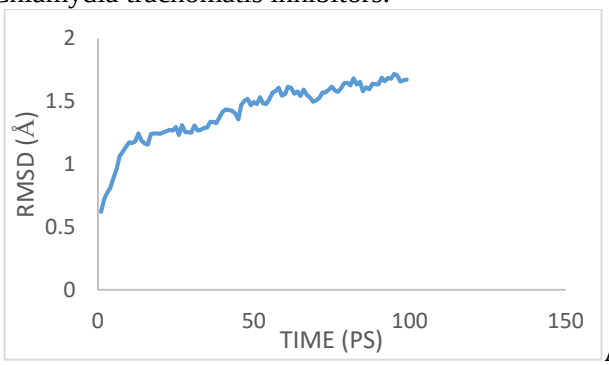

A

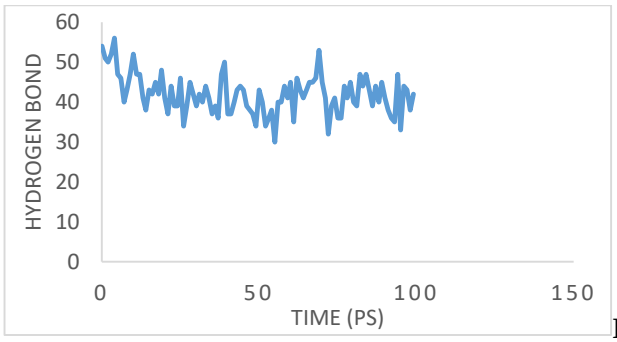

B

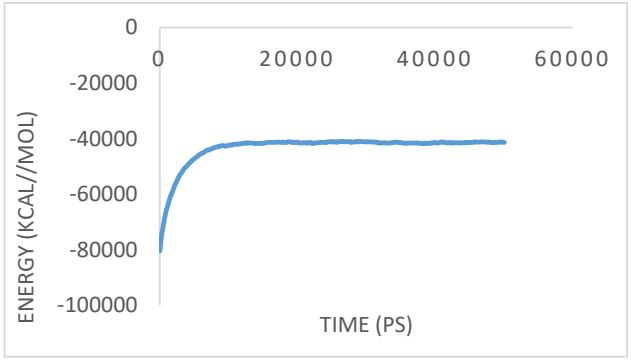

C

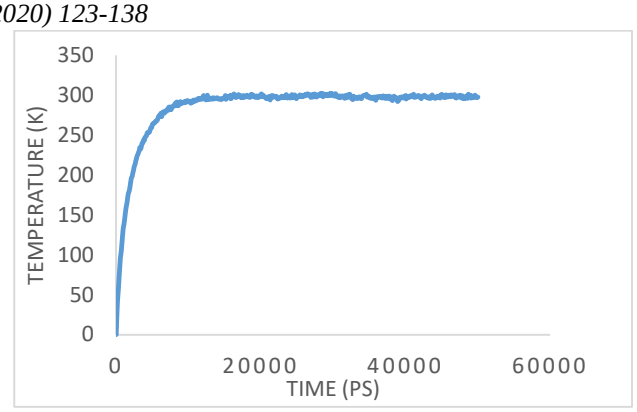

D

Figure 5. Simulated protein (A) RMSD of the protein; (B) Hydrogen bond of the protein; (C) Total energy of the protein and (D) Temperature of the simulated protein.

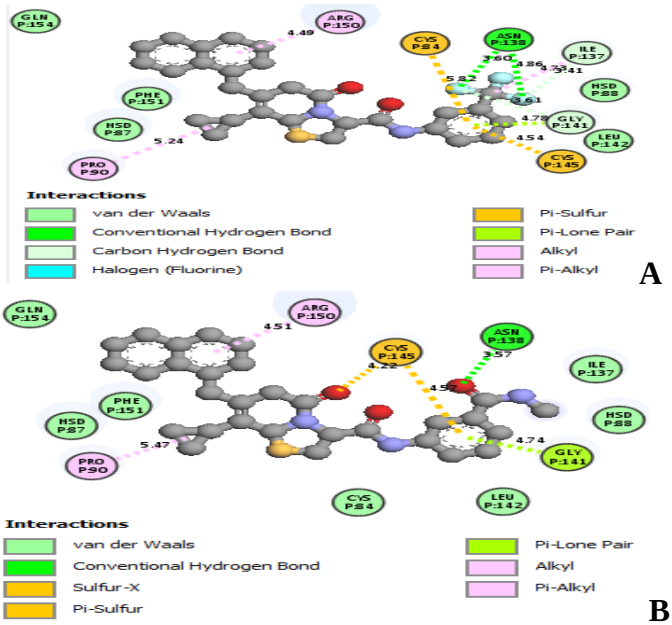

A

B

Figure 6. 2D simulated complex (A) compound 29 and (B) compound 31

According to Muegge and his coworker proposed that, for effective drug candidates, molecular weight (MW) should be less than 600 but greater than 200Da and the atomistic and knowledge-based method (XLOGP3) should be greater than -2 and less than 5 [33]. Golden triangles were applied according to Muegge et al., proposal. The Golden Triangle can be used as a device to affect the plan of new focuses by accomplishing a higher likelihood of drug-like space [34].

The likelihood of achievement in amplifying strength, steadiness, and penetrability is acknowledged by moving the plan properties into a region with a baseline of XLOGP3 = 2 to 7 at MW = 600, these cutoff points a three-sided shape (triangular shape), called the golden triangle. For our arrangement of molecules, compound 31 has an extraordinary vulnerability and low clearance since they are engaged inside the golden triangle area (Figure 8). As per the outcomes got by these principles, these compounds 31 (with MW = 509.62 and XLOGP4 = 4.28) have the most elevated likelihood of

accomplishment in augmenting intensity, stability, porousness, and oral ingestion compared to compound 29 (with MW = 520.57 and XLOGP3 = 5.89).

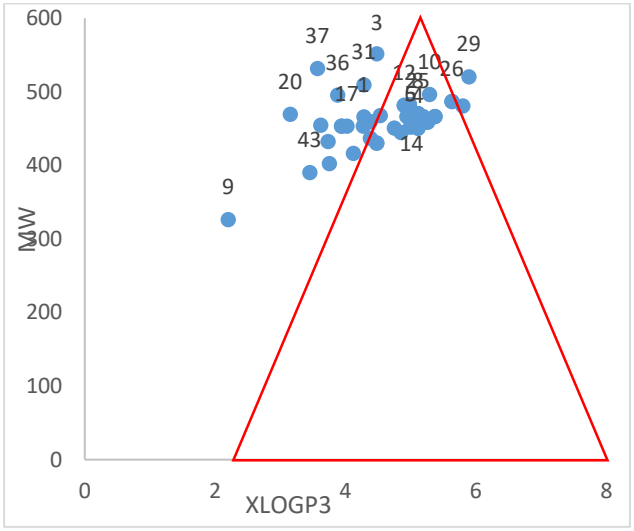

Figure 7. Permeability, potency, stability, and clearance trends across MW and XLOGP3.

3. Material and Methods

3.1. General

The dataset utilized in this investigation comprised of a series of thiazolino 2-pyridone amide derivative that has been reported as antimicrobial activity against Chlamydia trachomatis [https://pubchem.ncbi.nlm.nih.gov/bioassay/1293489]. The test IC_{50} estimations of all compounds in µM were changed over into pIC_{50} by taking -Log (IC50×10^-6) and were utilized as the reliant variable.

There were a total of 46 thiazolino 2-pyridone amide derivatives which are then part into a training set of 37 compounds for generating 2D and 3D QSAR models and a test set of 9 compounds for validating the nature of the models.

The compounds in the test set were manually selected from the original pool of structures based on activity/property-based. This methodology is based on activity (activity/property based) sampling. Molecules with low, moderate, and high activity were put in both sets for the maintenance of uniform distribution. Table 4 lists all of the names and related inhibitory behaviors. Using the freely available Marvin View program, 2D structures of 46 thiazolino 2-Pyridone amide derivatives were developed. Then the structures were translated to the format .sdf. To build a three dimensional (3D) structure, the .sdf file is transferred to Spartan'14 v1.1.4. These structures were then exposed to energy minimization. Energy-minimized molecules were exposed to streamlining through parameterization strategy (semi-empirical PM3). Finally, optimized with semi-empirical (PM6) and also transferred to PaDEL-Descriptor version 2.20 [13] and were subjected to a re-optimization MMFF94 force field.

Table 4: Thiazolino 2-pyridone amide analog compounds as Chlamydia trachomatis inhibitor

No.	NAME	CID	µM	pIC50	Binding Energy
1	6-amino-7-[(4-chlorophenyl) methyl]-8-cyclopropyl-N-(4-methylphenyl) -5-oxo-2,3-dihydrothiazolo[3,2-a]pyridine-3-carboxamide	127029110	2.5	5.6021	-7.7
2	6-amino-8-cyclopropyl-7-[(2,3-dimethylphenyl)methyl]-N-(4-methylphenyl) -5-oxo-2,3-dihydrothiazolo[3,2-a]pyridine-3-carboxamide	127029111	1	6	-7.1
3	(3R)-8-cyclopropyl-6-(4-morpholinylmethyl)-7-(1-naphthalenylmethyl)-5-oxo-N-phenyl-2,3-dihydrothiazolo[3,2-a]pyridine-3-carboxamide	127029112	5	5.3010	-7.9
4	8-cyclopropyl-7-(1-naphthalenylmethyl)-5-oxo-N-phenyl-3-thiazolo[3,2-a]pyridinecarboxamide	86280664	2.5	5.6021	-8.2
5	8-cyclopropyl-7-(1-naphthalenylmethyl)-5-oxo-N-	86344191	2.5	5.6021	-7.7

	phenyl-2,3-dihydrothiazolo[3,2-a]pyridine-3-carboxamide				
6	(3R)-8-cyclopropyl-7-(1-naphthalenylmethyl)-5-oxo-N-phenyl-2,3-dihydrothiazolo[3,2-a]pyridine-3-carboxamide	86344376	2.5	5.6021	-8.0
7	(3S)-8-cyclopropyl-7-(1-naphthalenylmethyl)-5-oxo-N-phenyl-2,3-dihydrothiazolo[3,2-a]pyridine-3-carboxamide	86344377	2.5	5.6021	-8.2
8	8-cyclopropyl-N-(2-fluorophenyl)-7-(1-naphthalenylmethyl)-5-oxo-2,3-dihydrothiazolo[3,2-a]pyridine-3-carboxamide	123794473	2.5	5.6021	-8.2
9	8-cyclopropyl-7-methyl-5-oxo-N-phenyl-2,3-dihydrothiazolo[3,2-a]pyridine-3-carboxamide	123731462	10	5	-7.0
10	3-[anilino(oxo)methyl]-8-cyclopropyl-7-(1-naphthalenylmethyl)-5-oxo-2,3-dihydrothiazolo[3,2-a]pyridine-6-carboxylic acid	127030009	10	5	-7.9
11	6-amino-8-cyclopropyl-7-(1-naphthalenylmethyl)-5-oxo-N-phenyl-2,3-dihydrothiazolo[3,2-a]pyridine-3-carboxamide	123282269	0.25	6.6021	-8.4
12	6-amino-8-cyclopropyl-N-(3-methylphenyl)-7-(1-naphthalenylmethyl)-5-oxo-2,3-dihydrothiazolo[3,2-a]pyridine-3-carboxamide	127030012	1	6	-8.7
13	6-amino-8-cyclopropyl-N-(4-methylphenyl)-7-(1-naphthalenylmethyl)-5-oxo-2,3-dihydrothiazolo[3,2-a]pyridine-3-carboxamide	127030013	0.25	6.6021	-7.9
14	8-cyclopropyl-7-[(2,3-dimethylphenyl)methyl]-5-oxo-N-phenyl-2,3-dihydrothiazolo[3,2-a]pyridine-3-carboxamide	123344660	2.5	5.6021	-7.7
15	8-cyclopropyl-7-[(2,3-dichlorophenyl)methyl]-5-oxo-N-phenyl-2,3-	127030039	2.5	5.6021	-7.8

	dihydrothiazolo[3,2-a]pyridine-3-carboxamide				
16	8-cyclopropyl-7-[(3,4-dimethylphenyl)methyl]-5-oxo-N-phenyl-2,3-dihydrothiazolo[3,2-a]pyridine-3-carboxamide	1239087888	2.5	5.6021	-7.6
17	8-cyclopropyl-5-oxo-N-phenyl-7-(5-quinolinylmethyl)-2,3-dihydrothiazolo[3,2-a]pyridine-3-carboxamide	1270303333	10	5	-8.0
18	8-cyclopropyl-7-[(2,3-dimethylphenyl)methyl]-N-(4-methylphenyl)-5-oxo-2,3-dihydrothiazolo[3,2-a]pyridine-3-carboxamide	1270303334	1	6	-7.8
19	7-[(4-chlorophenyl)methyl]-8-cyclopropyl-N-(4-methylphenyl)-5-oxo-2,3-dihydrothiazolo[3,2-a]pyridine-3-carboxamide	1270303335	1	6	-7.1
20	6-amino-8-cyclopropyl-7-(1-naphthalenylmethyl)-5-oxo-N-(4-pyrimidinyl)-2,3-dihydrothiazolo[3,2-a]pyridine-3-carboxamide	1270306301	2.5	5.6021	-8.3
21	8-cyclopropyl-5-oxo-N-phenyl-7-(phenylmethyl)-2,3-dihydrothiazolo[3,2-a]pyridine-3-carboxamide	1237558201	2.5	5.6021	-7.5
22	8-cyclopropyl-7-[(3-methylphenyl)methyl]-5-oxo-N-phenyl-2,3-dihydrothiazolo[3,2-a]pyridine-3-carboxamide	1270306311	2.5	5.6021	-7.7
23	7-[(4-chlorophenyl)methyl]-8-cyclopropyl-5-oxo-N-phenyl-2,3-dihydrothiazolo[3,2-a]pyridine-3-carboxamide	1270306321	2.5	5.6021	-6.9
24	8-cyclopropyl-7-[(4-methoxyphenyl)methyl]-5-oxo-N-phenyl-2,3-dihydrothiazolo[3,2-a]pyridine-3-carboxamide	1270306331	2.5	5.6021	-7.4
25	8-cyclopropyl-N-(3-fluorophenyl)-7-(1-naphthalenylmethyl)-5-oxo-2,3-dihydrothiazolo[3,2-a]pyridine-3-carboxamide	1239419231	2.5	5.6021	-8.4

26	N-(3-chlorophenyl)-8-cyclopropyl-7-(1-naphthalenylmethyl)-5-oxo-2,3-dihydrothiazolo[3,2-a]pyridine-3-carboxamide	12390916 0	2.5	5.6021	-8.2
27	8-cyclopropyl-N-(3-methylphenyl)-7-(1-naphthalenylmethyl)-5-oxo-2,3-dihydrothiazolo[3,2-a]pyridine-3-carboxamide	86345111	1	6	-8.4
28	8-cyclopropyl-N-(3-ethylphenyl)-7-(1-naphthalenylmethyl)-5-oxo-2,3-dihydrothiazolo[3,2-a]pyridine-3-carboxamide	12705338 3	2.5	5.6021	-8.2
29	8-cyclopropyl-7-(1-naphthalenylmethyl)-5-oxo-N-[3-(trifluoromethyl)phenyl]-2,3-dihydrothiazolo[3,2-a]pyridine-3-carboxamide	12370150 8	2.5	5.6021	-8.9
30	8-cyclopropyl-N-(3-methoxyphenyl)-7-(1-naphthalenylmethyl)-5-oxo-2,3-dihydrothiazolo[3,2-a]pyridine-3-carboxamide	12337572 4	2.5	5.6021	-8.1
31	8-cyclopropyl-N-[3-(methylcarbamoyl)phenyl]-7-(1-naphthalenylmethyl)-5-oxo-2,3-dihydrothiazolo[3,2-a]pyridine-3-carboxamide	12705339 0	10	5	-8.9
32	8-cyclopropyl-N-(4-fluorophenyl)-7-(1-naphthalenylmethyl)-5-oxo-2,3-dihydrothiazolo[3,2-a]pyridine-3-carboxamide	12383049 4	2.5	5.6021	-7.9
33	N-(4-chlorophenyl)-8-cyclopropyl-7-(1-naphthalenylmethyl)-5-oxo-2,3-dihydrothiazolo[3,2-a]pyridine-3-carboxamide	12387665 3	2.5	5.6021	-8.0
34	8-cyclopropyl-N-(4-methylphenyl)-7-(1-naphthalenylmethyl)-5-oxo-2,3-dihydrothiazolo[3,2-a]pyridine-3-carboxamide	11771050 9	2.5	5.6021	-8.0

35	8-cyclopropyl-N-(4-methoxyphenyl)-7-(1-naphthalenylmethyl)-5-oxo-2,3-dihydrothiazolo[3,2-a]pyridine-3-carboxamide	12359598 3	2.5	5.6021	-8.2
36	N-(4-carbamoylphenyl)-8-cyclopropyl-7-(1-naphthalenylmethyl)-5-oxo-2,3-dihydrothiazolo[3,2-a]pyridine-3-carboxamide	12328833	2.5	5.6021	-8.0
37	8-cyclopropyl-7-(1-naphthalenylmethyl)-5-oxo-N-(4-sulfamoylphenyl)-2,3-dihydrothiazolo[3,2-a]pyridine-3-carboxamide	12352025 0	10	5	-8.2
38	8-cyclopropyl-7-(1-naphthalenylmethyl)-5-oxo-N-(2-pyridinyl)-2,3-dihydrothiazolo[3,2-a]pyridine-3-carboxamide	12362570 0	10	5	-7.9
39	8-cyclopropyl-7-(1-naphthalenylmethyl)-5-oxo-N-(3-pyridinyl)-2,3-dihydrothiazolo[3,2-a]pyridine-3-carboxamide	12368818 8	10	5	-7.8
40	8-cyclopropyl-7-(1-naphthalenylmethyl)-5-oxo-N-pyridin-4-yl-2,3-dihydrothiazolo[3,2-a]pyridine-3-carboxamide	12377057 3	5	5.3010	-7.6
41	8-cyclopropyl-7-(1-naphthalenylmethyl)-5-oxo-N-(4-pyrimidinyl)-2,3-dihydrothiazolo[3,2-a]pyridine-3-carboxamide	12401743 2	2.5	5.6021	-8.2
42	8-cyclopropyl-7-(1-naphthalenylmethyl)-5-oxo-N-(2-thiazolyl)-2,3-dihydrothiazolo[3,2-a]pyridine-3-carboxamide	12400303 9	5	5.3010	-7.7
43	8-cyclopropyl-N-methyl-7-(1-naphthalenylmethyl)-5-oxo-2,3-dihydrothiazolo[3,2-a]pyridine-3-carboxamide	12705342 1	10	5	-7.4

44	N-cyclohexyl-8-cyclopropyl-7-(1-naphthalenylmethyl)-5-oxo-2,3-dihydrothiazolo[3,2-a]pyridine-3-carboxamide	12356746 5	10	5	-7.6
45	8-cyclopropyl-7-(1-naphthalenylmethyl)-5-oxo-N-(phenylmethyl)-2,3-dihydrothiazolo[3,2-a]pyridine-3-carboxamide	12340547 6	2.5	5.6021	-8.0
46	8-cyclopropyl-N-methyl-7-(naphthalen-1-ylmethyl)-5-oxo-N-phenyl-2,3-dihydro-[1,3]thiazolo[3,2-a]pyridine-3-carboxamide	12340343 1	5	5.3010	-8.4

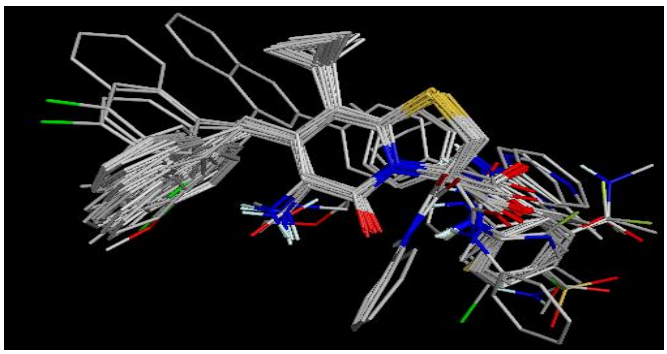

Figure 8. Alignment of thiazolino 2-pyridone amide inhibitors as obtained from Open3DALIGN

3.2. 2D-QSAR and CoMFA analysis

Physicochemical properties are the mathematical description of a comprising numerous sources of transformed and coded chemical knowledge to address chemical, biological, and pharmacological issues. Various physicochemical descriptors for each of the compounds in the dataset using PaDEL software v2.20 [13] are determined for the creation of 2D QSAR models. Various arrangements of 2D and 3D molecular descriptors are determined with the assistance of PaDEL software. Using DTC-Lab software (http://poi.apache.org/), 2D-QSAR models were developed. The stepwise multiple linear regression (S-MLR) is utilized to assemble the QSAR model. The basic idea behind the stepwise MLR regression approach is that by entering and removing predictors in a stepwise way until there is no justifiable reason to enter or remove any more to construct a multiple linear regression (MLR) model from a collection of predictors/independent variables/descriptors, i.e. till no more significant variable is available.

One of the most important steps for obtaining a correct molecular interaction field model is the sufficient alignment of the compounds relative to each other in the 3D-QSAR analysis. Energy-minimized molecular structures were aligned using the template-based process. In the combination of Atom-based fashion and pharmacophore-based fashion, the mixed alignment process was performed using Open3DALIGN software v2.3, an open-source platform capable of performing 3D molecular structures' multi-conformational, unsupervised rigid-body alignment [14]. Using all available molecules as potential templates, the alignment procedure was carried out. Therefore, 46 alignments, each obtained by superimposition on the corresponding molecule of the template, were made. An O3A-score derived from the source code of the Open3DALIGN software is measured for each alignment, which indicates the consistency of the superimposition. For further study, the alignment corresponding to the highest cumulative O3A-score has been chosen. Figure 8 reveals the optimal alignment under which the prototype was chosen as compound 29.

CoMFA (Comparative Molecular Field Analysis) is an adjustable tool for quantitatively describing 3D-QSAR. This analysis utilized Open3DQSAR to perform CoMFA investigation which is an open-source program available for high-throughput molecular interaction force field (MIF) chemometric analysis [15]. The best arrangement with compound 29 as a format is put in a three-dimensional (3D) cubic lattice with a grid size of 2Å and a distance of 5.0Å. Using an sp3 hybridized carbon atom probe with + 1 charge, van der Waals' (steric fields) were computed. Similarly, using a volume less probe, electrostatic fields were computed. Such energies of steric and electrostatic interaction were regarded as independent variables (CoMFA descriptors). To minimize the noise concealed in the partial least square (PLS) matrix and thus decrease the computational time, the CoMFA model was developed following pre-treatment operations:

(1) A cutoff value of −30.0 and +30.0 kcal/mol respectively was set for the minimum and maximum steric and electrostatic energy values. The infinity of

energy values within the molecule is avoided by this pretreatment.

2) For both probes, it zeroes both negative and positive values below a threshold of 0.05.

3) Eliminates X variables below a threshold of 0.1 with a Standard Deviation.

4) N-level variables are variables that presume that only N values have been removed from the training set, most of which are spread over a limited number of items. This mechanism prevents the importance of unique substituents found in a single molecule from overweighting. Otherwise, the entire model may be adversely influenced by it.

5) The entire block of X or Y variables, scaled by the technique of block unscaled weighting (BUW). Reasonable variable clustering and selection processes such as smart region description (SRD) and fractional factorial design (FFD) will significantly boost the CoMFA model's predictivity. With no predictability, these variable selection strategies selectively delete noisy variables. Based on their closeness in 3D space, the SRD procedure performs variable grouping to reduce the redundancy resulting from the presence of several nearby descriptors that mainly encode the same type of information [16]. FFD seeks to select variables that increase predictive ability significantly (using the paradigms of LOO) and can operate on both single variables or groups identified by a previous SRD run, thereby eliminating groups of uninformative variables as performed in GOLPE [17]. To achieve a connection between the descriptors derived from CoMFA (independent variables) and pIC50 values, PLS analysis implemented in Open3DQSAR was used to (dependent variable). Through the Non-linear iterative partial least squares (NIPALS) algorithm [18], Open3DQSAR generates a PLS model. The overall significance of the model was determined by statistical parameters such as the determination coefficient (R2), Standard Deviation Error in Estimation (SDEC), Standard Deviation Error in Predictivity (SDEP), and the F-ratio measure. Also, for the steric and electrostatic fields, the CoMFA color contour maps are derived.

3.3. Docking Decorum

The docking of ligands to protein complex was performed using Auto Dock/vina software using PyRx as GUI [19]. The three dimensional (3D) x-ray crystal structure of chlamydia trachomatis DsbA (PDB ID: 5KBC) was recovered from RCSB PDB (https://www.rcsb.org/structure/5kbc). The water particles just as co-solidified ligands were removed from the PDB file. The protein was loaded in software and it was prepared for docking. During this process, the protein will be transformed from .pdb format to .pdbqt format, a format needed for Auto Dock/vina for docking. Similarly, the derivatives (optimized ligands) were also loaded and were changed over to the .pdbqt format. Before docking, the grid box was placed around the binding site so as enable the ligands to bind only inside the grid box i.e., in the binding site. After the grid box was set, the docking simulations were run for all the ligands. The Auto Dock/vina calculates the energy values using the Lamarckian Genetic Algorithm (LGA) algorithm. A total of ten binding configurations was generated for each ligand and were arranged according to their root mean square deviation (RMSD) values. The binding confirmation ranked one with an RMSD of zero was selected as the best in terms of binding energy and pose.

3.4. Enzyme grid generation

The ligand was held in the crystal structure of the readied protein which was used for the enzyme grid generation. The coupling box measurements of the protein was set to exhaustiveness = 8; center_x = -1.1386; center_y = 27.2208; center_z = -1.7311; size_x = 52.1493; size_y = 44.4336 and size_z = 54.8482. The output .pdbqt collections were written into a configuration (conf) file. The enzyme was treated as an inflexible entity whereas ligands were kept adaptable to accomplish the best fitting confirmation concerning the enzyme/receptor complex. The coupling compliance of ligands with the least restricting proclivity was portrayed as the steadiest adaptation of the ligands to the receptor. The binding conformation of ligands with the lowest binding affinity was characterized as the most stable conformation of the ligands to the receptor. The visualization tools using discovery studio visualizer v17.2 were employed to analyze intermolecular chemical interactions such as hydrogen bonding, ionic interactions, and hydrophobic contacts, and so on.

*3.5. Molecular Dynamics (MD) Simulations*Calculations of molecular dynamics (MDs) simulations are conducted using VMD [20] and NAMD [21] and CHARMM force field [22]. Interaction parameters have been calculated using the CHARMM27 force field (par_all27_prot_lipid.inp). The protein was solvated and was dissolved with explicit water at a concentration of 0.15mol/L NaCl salt for neutralization. Minimization was performed to simplify the original protein structure. To confirm the structure to the force field [23], the application of solvents and, in particular, to minimize steric clashes that may occur in the device [24]. To perform the simulation, this procedure supplied the computer with the lowest energy. The solvated framework was minimized first for 50000 steepest plunge technique cycles. After the minimization, it was characterized by the achievement of energy convergence. From that point onward, the device temperature was steadily heated from 0 K to 310 K in 100ps. At the end of the day, the system was calibrated at 310 K for 100ps with the NVT ensemble. On the DELL; Intel ® Core ™ i5 CPU M 540 @ 2.53 GHz and 4GB RAM, 64-bit-Operating System, x64-based CPU, the MD simulation,

and analysis results were conducted. In the NAMD documentation (www.ks.uiuc.edu /Research/namd/), a full summary of the input parameters is given. See (www.ks.uiuc.edu/Research/namd /current /ug/) for more detail on running MD simulations with NAMD.

4. Conclusion

The principles and methods discussed in this research highlight the strategies by which 2D-3D QSAR, molecular docking, and molecular dynamic simulation approaches have been applied in the identification of novel bioactive compounds. Our present studies have established that the structural features and binding mechanism of compound 29 and 31 through Molecular Interaction Force Fields (MIFs) studies are quite reliable and significant. The CoMFA (UVEPLS) studies indicate that the steric and electrostatic interaction plays an important role in determining the potency of the compounds. Docking on the same simulated A-chain of protein reveals that the ligand (compound 29 and 31) is bonded to conventional hydrogen bonds, electrostatics, and hydrophobic interaction (such as pi-sulfur, pi-alkyl, and pi-pi t-shaped). Moreover, the ligand-protein complex was used in MD simulation to realize the conformation changes of the complex. The total energy, temperature, and root mean square deviation (RMSD) plot revealed that the complex (compound 31) was stable and the conformation of the ligand-protein complex has a slight change relative to the protein conformation. From the above methods, compound 31 with a molecular weight of 509.62 and XLOGP4 of 4.28 have stronger potency, stability, permeability, and oral absorption compared to compound 29 with a molecular weight of 520.57 and XLOGP3 of 5.89. From these studies, we have added valuable information into the factors governing the potency of the Chlamydia trachomatis inhibitors.

Acknowledgements

The authors gratefully acknowledge the Department of Chemistry, Ahmadu Bello University, Zaria (Samaru, Zaria-Nigeria); for computational studies, and as part of the Ph.D. thesis.

References

[1] S. Marwaha, H. Uvell, O. Salin, A. E. G. Lindgren, J. Silver, M. Elofsson, A. Gylfe, N-acylated Derivatives of Sulfamethoxazole and Sulfafurazole Inhibit Intracellular Growth of Chlamydia trachomatis. Antimicrobial Agents and Chemotherapy 58(5) (2014) 2968–2971.

[2] B.E. Batteiger, "Chlamydia infection and epidemiology," in Intracellular Pathogens I: Chlamydiales, eds M. Tan, and P. Bavoil (Washington, DC: ASMpress), 1–26 (2012).

[3] P. Engström, S. Krishnan, B.D. Ngyuen, E. Chorell, J. Normark, J. Silver, R.J. Bastidas, M.D. Welch, S.J. Hultgren, H. Wolf-Watz, R.H. Valdivia, F. Almqvist, S. Bergström, A 2-pyridone-amide inhibitor targets the glucose metabolism pathway of Chlamydia trachomatis. mBio 6(1):e02304-14 (2015). doi:10.1128/mBio.02304-14.

[4] WHO (2018). Trachoma: Fact Sheet. World Health Organization. Available online at http://www.who.int/news-room/fact-sheets/detail/trachoma (Accessed September 30, 2020).

[5] L. Newman, J. Rowley, S. Vander Hoorn, N. S. Wijesooriya, M. Unemo, N. Low, G. Steven, S. Gottlieb, J. Kiarie, M. Temmerman, Global estimates of the prevalence and incidence of four curable sexually transmitted infections in 2012 based on systematic review and global reporting. PLoS ONE (2015) Dec 8;10(12):e0143304.

[6] A. Balupuri, P.K. Balasubramanian, S. J. Cho. 3D-QSAR, docking, molecular dynamics simulation and free energy calculation studies of some pyrimidine derivatives as novel JAK3 inhibitors. Arabian Journal of Chemistry 13, (2020) 1052–1078.

[7] K. Zitouni, S. Belaidi, A. Kerassa, Conformational analysis and QSAR modeling 14-membered macrolide analogues against mycobacterium tuberculosis. J Fundam Appl Sci., 12(3), (2020) 1035-1066.

[8] M.K. Dahlgren, C. E. Zetterström, A. Gylfe, A. Linusson, M. Elofsson. Statistical molecular design of a focused salicylidene acylhydrazide library and multivariate QSAR of inhibition of type III secretion in the Gram-negative bacterium Yersinia. Bioorg. Med. Chem. 18 (2010) 2686–2703.

[9] S.A. Mojica, A.U. Eriksson, R.A. Davis, W. Bahnan, M. Elofsson, A. Gylfe, Red Fluorescent Chlamydia trachomatis Applied to Live Cell Imaging and Screening for Antibacterial Agents. Front. Microbiol. 9 (2018) 3151. doi: 10.3389/fmicb.2018.0315.

[10] C. A. Ison, Antimicrobial resistance in sexually transmitted infections in the developed world: implications for rational treatment. Curr. Opin. Infect. Dis. 25 (2012) 73–78.

[11] E. Bojang, J. Jafali, V. Perreten, J. Hart, E.M. Harding-Esch, A. Sillah, D.C.W. Mabey, M.J. Holland, R.L. Bailey, A. Roca, S.E. Burr, Short-term increase in prevalence of nasopharyngeal carriage of macrolide-resistant Staphylococcus aureus following mass drug administration with azithromycin for trachoma control. BMC Microbiol. 17 (2017) 75.

[12] M. R. Hammerschlag, S. A. Kohlhoff, Treatment of chlamydial infections. Expert Opin. Pharmacother. 13, 545–552 . (2012).

[13] C.W. Yap, PaDEL-descriptor: An open-source software to calculate molecular descriptors and fingerprints. Journal of Computational Chemistry, 32 (7) 1466-1474 (2011).

[14] P. Tosco, T. Balle, F. Shiri, Open3DALIGN: an open-source software aimed atunsupervised ligand alignment, J. Comput. Aided Mol. Des. 25 777–783 (2011).

[15] P. Tosco, T. Balle, Open3DQSAR: a new open-source software aimed athigh-throughput chemometric analysis of molecular interaction fields, J. Mol.Model. 17 201–208 (2011).

[16] M. Pastor, G. Cruciani, S. Clementi, Smart region definition: a new way toimprove the predictive ability and

interpretability of three-dimensional quantitative structure-activity relationships, J. Med. Chem. 40 1455–1464 (1997).
[17] S.C. Massimo Baroni, Gabriele Costantino, Gabriele Cruciani, Daniela Riganelli,Roberta Valigi, Generating optimal linear PLS estimations (GOLPE): anadvanced chemometric tool for handling 3D-QSAR problems, Quant. Struct. Relat. 12 9–20 (1993).
[18] S. Wold, M. Sjöström, L. Eriksson, PLS-regression: a basic tool ofchemometrics, Chemometr. Intell. Lab. Syst. 58 (2001) 109–130.
[19] G. Morris, R. Huey, AutoDock4 and AutoDockTools4: Automated docking with selective receptor flexibility, J .Comput. Chem. 30 (2009) 2785–2791.
[20] W. Humphrey, A. Dalke, K. Schulten, VMD: Visual Molecular Dynamics. J Mol Graph 7855 (1996) 33–38.
[21] J.C. Phillips, R. Braun, W. Wang, J. Gumbart, E. Tajkhorshid, E. Villa, C. Chipot, R.D. Skeel, L. Kale, K Schulten, Scalable molecular dynamics with NAMD. J. Comput. Chem. 26 (2005) 1781–1802, doi.org/10.1002/jcc.20289. A.D. MacKerell, D. Bashford, M. Bellott, R.L. Dunbrack, J.D. Evanseck, M.J. Field, S.
[22] J. Fischer, H. Gao, S. Guo, D. Ha, L. Joseph-McCarthy, L. Kuchnir, K. Kuczera, F.T. Lau, C. Mattos, S. Michnick, T. Ngo, D.T. Nguyen, B. Prodhom, W.E. Reiher, B. Roux, M. Schlenkrich, J.C. Smith, R. Stote, J. Straub, M. Watanabe, J. Wiórkiewicz-Kuczera, D. Yin, M. Karplus, All atom empirical potential for molecular modeling and dynamics studies of proteins. J Phys Chem B. 102(18) (1998) 3586-616.
[23] A.K.L. Wong, A. M. Goscinski, A VMD plugin for NAMD simulations on Amazon EC2. Procedia Computer Science, 9, (2012) 136-145.
[24] A. K. L. Wong, A.M. Goscinski, The design and implementation of the VMD plugin for NAMD simulations on the Amazon cloud. International Journal of Cloud Computing and Services Science, 1(4), (2012) 155.
[25] A. Golbraikh, A. Tropsha, Beware of q2! J Mol Graph Model. 20 (2002) 269-276. [26]
[26] S.E. Abechi, and E.I. Edache, Application of genetic algorithm-multiple linear regression (GA-MLR) for prediction of anti-fungal activity. International Journal of Pharma Sciences and Research (IJPSR) 7 (2016) 204-220.
[27] P.P. Roy, K. Roy, On some aspects of variable selection for partial least squares regression models. QSAR Comb Sci. 27 (2008) 302-313
[28] P. Gramatica and E. Papa, Screening and Ranking of POPs for Global Half-Life: QSAR Approaches for Prioritization Based on Molecular Structure. Environ. Sci. Technol. 41, (2007) 2833-2839. doi.org/10.1021/es061773b.
[29] S. Cassani, P. Gramatica, Identification of potential PBT behavior of personal care products by structural approaches. Sustainable Chemistry and Pharmacy 1 (2015) 19-27.
[30] E.I. Edache, A.J. Uttu, A. Oluwaseye, H. Samuel, and A. Abduljelil, A Semi-empirical based QSAR study of indole ***β***- Diketo acid, Diketo acid and Carboxamide Derivatives as potent HIV-1 agent Using Quantum Chemical descriptors. IOSR Journal of Applied Chemistry (IOSR-JAC), 8 (2015) 12-20
[31] S. Shapiro, B. Guggenheim, Inhibition of oral bacteria by phenolic compounds: Part 1. QSAR analysis using molecular connectivity. Quant. Struct. Act Relat. 17 (1998) 327-337.
[32] B. Wendt, R.D. Cramer, Challenging the gold standard for 3DQSAR: template CoMFA versus X-ray alignment. J Comput Aided Mol Des 28(8) (2014) 803–824.
[33] I. Muegge, S. L. Heald, and D. Brittelli, Simple Selection Criteria for Drug-like Chemical Matter. Journal of Medicinal Chemistry 44 (12) (2001) 1841-1846.
[34] T.W. Johnson, K.R. Dress, M. Edwards, Using the Golden Triangle to optimize clearance and oral absorption. Bioorg. Med. Chem. Lett. 19 (2009) 5560–5564.

How to Cite This Article

Emmanuel I Edache; Adamu I Uzairu; Paul Andrew Mamza; Gideon Adamu Shallangwa. "Computational Modeling and Molecular dynamics Simulations of Thiazolino 2-pyridone amide analog compounds as Chlamydia trachomatis inhibitor". Journal of Chemistry Letters, 1, 3, 2020, 123-138. doi: 10.22034/jchemlett.2021.262437.1011